

Effect of Non-magnetic Ions Substitution on Structural, Magnetic and Optical Properties of BiFeO₃ Nanoparticles

Manisha Arora · Sunil Chauhan · P. C. Sati ·
Manoj Kumar

Received: 12 December 2013 / Accepted: 14 February 2014 / Published online: 12 March 2014
© Springer Science+Business Media New York 2014

Abstract Non-magnetic Zr⁴⁺ ions substituted BiFeO₃ nanoparticles (BiFe_{1-x}Zr_xO₃, x = 0.0, 0.03 and 0.10) were synthesized by sol-gel method. X-ray diffraction and Raman studies indicate the rhombohedral phase for all the samples. The particle size decreases with increasing Zr⁴⁺ concentration and varies in the range 20–50 nm. The absorption spectra show the strong absorption of visible light with optical band gap variation 2.27–2.21 eV for pure and Zr-doped BFO nanoparticles. A large saturation magnetization value of 9.33 emu/g is observed for x = 0.03 sample. The reduction in saturation magnetization for x = 0.10 sample is attributed to the dominant role of an increasing number of non-magnetically active Zr⁴⁺ ions, and the formation of Fe–O–Zr coordination with increasing Zr⁴⁺ ions concentration becomes less magnetic sublattice.

Keywords Bismuth ferrite · Structural characterization · Magnetic properties · Optical properties

1 Introduction

In the recent years, there has been an increasing interest in magnetoelectric multiferroic materials, which show two ferroic properties such as spontaneous ferroelectric and magnetic ordering within the same phase. These materials have attracted great attention in the field of material science because of their potential applications in information storage, sensors, actuators and other memory devices [1]. BiFeO₃ (BFO) is one of the most candidate material

amongst all the multiferroic materials which combines both ferroic properties, i.e. antiferromagnetism ($T_N = 370$ °C) and ferroelectricity ($T_c = 810$ °C) in the same phase, having distorted rhombohedral perovskite structure (space group $R3c$) [2, 3]. Magnetic ordering in BFO is G-type antiferromagnetic (AFM) in which the superimposition of spatial spin modulation of periodicity ~ 62 nm driven by Dzyaloshinsky-Moriya (DM) interaction prevents the observation of weak ferromagnetic behaviour [4]. There are many reports on Bi-site substitution with La-, Nd- [5, 6] and Fe-site substitution with Ti and Mn to improve the multiferroic properties of BFO [7, 8]. Recently, Zr⁴⁺-doped [9] and Pr³⁺- and Zr⁴⁺ [10]-codoped BFO ceramics have shown the enhanced magnetic properties. Further, the optical properties are a relatively less explored area for BFO. Until to date, there are no reports on Zr-doped BFO nanoparticles and its magnetic and optical properties to the best of our knowledge. In the present communication, we report the synthesis, structural, magnetic and optical properties of Zr-doped BFO nanoparticle.

2 Experimental

2.1 Materials and Synthesis

Nanoparticles of Zr-doped BFO (BiFe_{1-x}Zr_xO₃ with x = 0.0, 0.03 and 0.10) were prepared by the sol-gel route. Bi(NO₃)₃·5H₂O, Fe(NO₃)₃·9H₂O and ZrO(NO₃)₂·xH₂O as starting materials and tartaric acid as a chelating agent were used to prepare Zr-doped BFO nanoparticles. The detailed processes for the preparation of the compositions are described elsewhere [11]. Hence, prepared gels were calcined at 550 °C for 2 h to get the desired phase. Phase identification and purity of the samples

M. Arora · S. Chauhan · P. C. Sati · M. Kumar (✉)
Department of Physics and Materials Science and Engineering,
Jaypee Institute of Information Technology, Noida 201307, India
e-mail: mkumar.phy@gmail.com

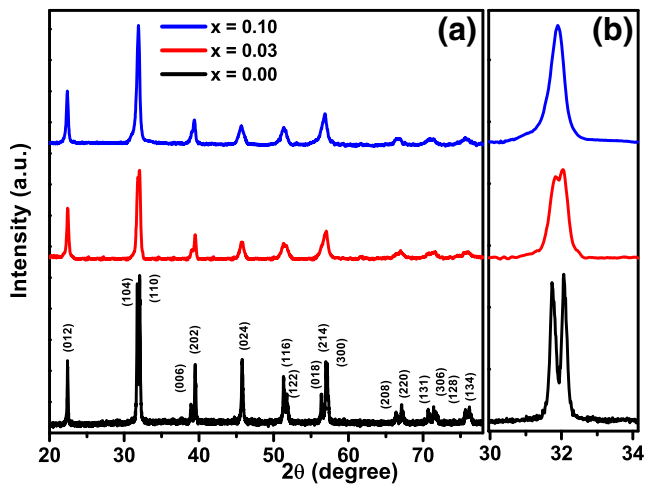


Fig. 1 **a** X-ray diffraction patterns of Zr-doped BFO nanoparticles and **b** enlarge view of diffraction peaks around $2\theta = 32^\circ$

was analysed by using an X-ray diffractometer (Bruker D8 Advanced). Transmission electron microscopy (TEM) images and selected area electron diffraction (SAED) pattern were taken on Philips CM10 in order to analyse particle size and crystallinity of the samples. Raman spectra were recorded on Renishaw Raman spectrometer by using 514.5-nm argon ion laser. The magnetic properties of the samples were measured by using a superconducting quantum interference device (SQUID). UV-visible diffuse reflectance

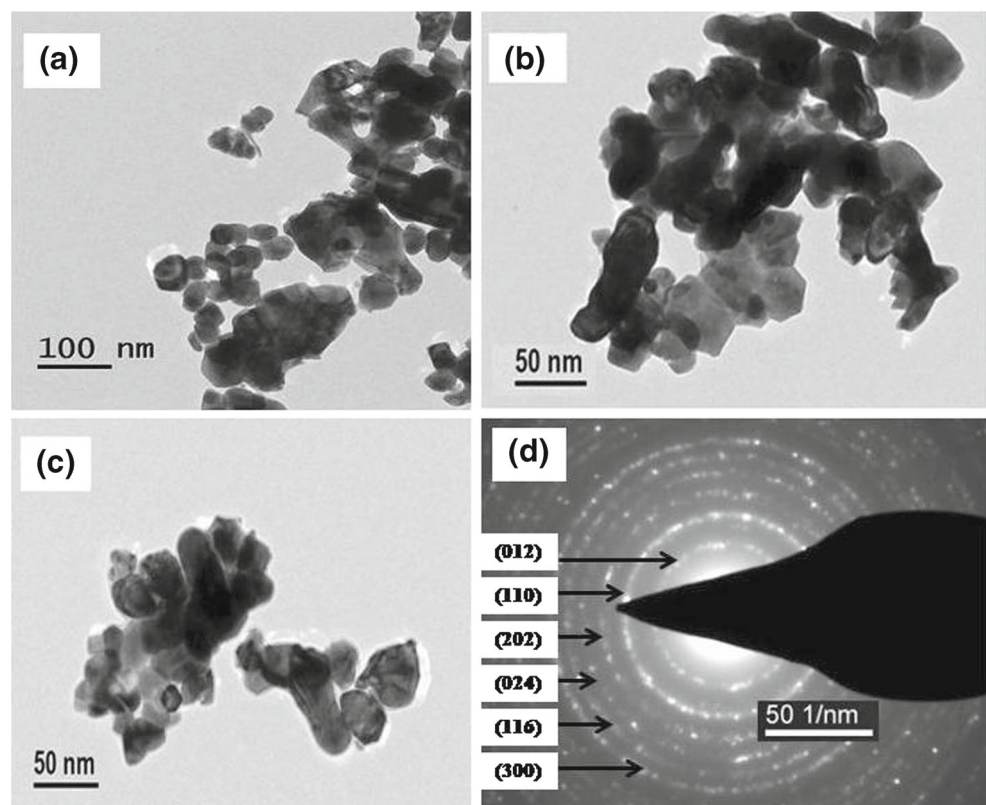
spectra were recorded on an Analytik Jena SPECORD 205 spectrometer.

3 Results and Discussion

3.1 X-ray Diffraction Analysis

Figure 1 shows the X-ray diffraction (XRD) patterns of pure and doped BFO nanoparticles with varying Zr concentrations. The phase formation without any trace of impurity has been observed for all samples. The XRD pattern of pure BFO sample shows the typical peaks of rhombohedral structure (JCPDS card number 71-2494). The distinguishable peaks from (006) and (202) planes around 2θ values of 39° are observed in all samples. However, with an increasing Zr concentration in $x = 0.03$ and 0.10 samples, there is a tendency of some peaks to merge. The peaks from (104) and (110) planes around 2θ values of 32° merged into a single peak for $x = 0.10$ sample (Fig. 1b). The merging of peaks indicates the distortion in the rhombohedral structure. However, the structural phase transformation is inevident up to $x = 0.10$ sample. Similar structural behaviour has already been reported in a Zr-doped BFO thin film [12]. The obtained lattice parameters are as follows: $a = b = 5.578 \text{ \AA}$, $c = 13.865 \text{ \AA}$; $a = b = 5.588 \text{ \AA}$, $c = 13.840 \text{ \AA}$; and $a = b = 5.604 \text{ \AA}$, $c = 13.854 \text{ \AA}$, for

Fig. 2 TEM images confirming formation of nanoparticles for **a** $x = 0.0$, **b** $x = 0.03$ and **c** $x = 0.10$ samples. **d** SAED pattern for $x = 0.0$ sample



$x = 0.0, 0.03$ and 0.10 samples, respectively. The average crystallite size as calculated using the Debye-Scherrer formula was found to be 40, 30 and 26.5 nm for $x = 0.0, 0.03$ and 0.10 samples, respectively, assuming that small crystallite size to be the only reason for line broadening of XRD peaks.

3.2 TEM Studies

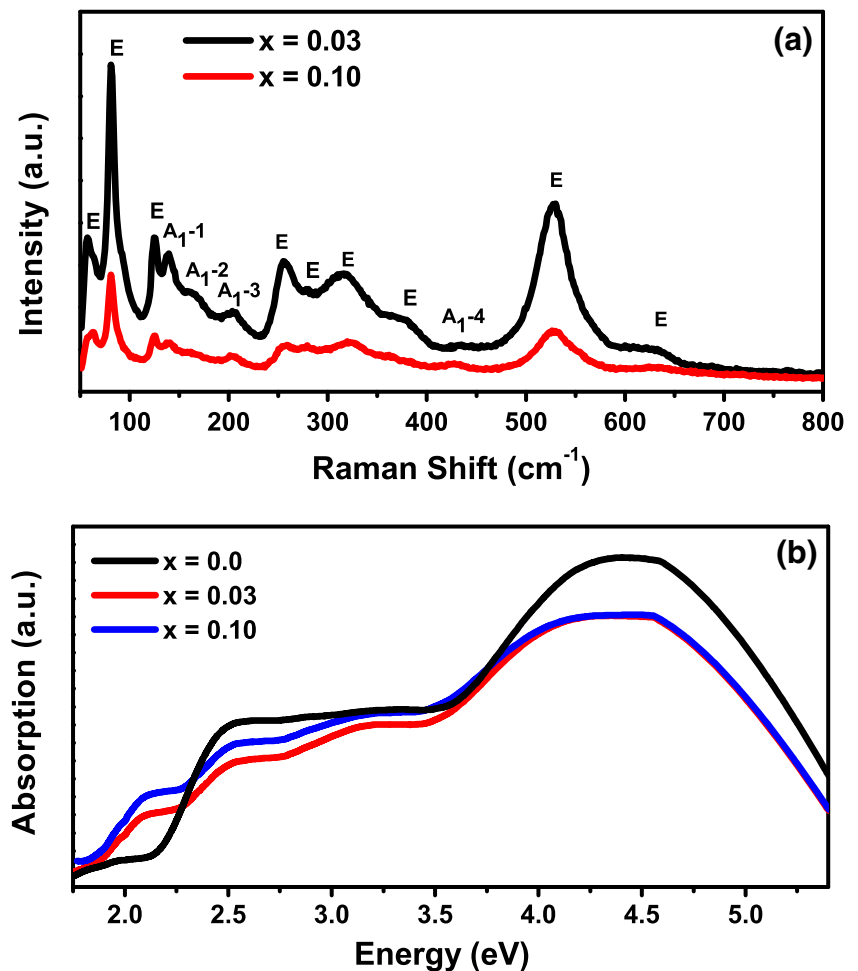
Transmission electron microscopy images confirming the formation of nanoparticles for $x = 0.0, 0.03$ and 0.10 samples are shown in Fig. 2a–c. TEM micrographs indicate that the average particle size decreases with an increasing Zr concentration in the samples. The average particle size observed from TEM images is 40, 35 and 30 nm for $x = 0.0, 0.03$ and 0.10 samples, respectively, with quasi-spherical morphology. Figure 2d shows the SAED pattern for $x = 0.0$ sample, indicating nice dot pattern that obviously display vastly crystalline nature of BFO nanoparticles. All

the diffraction rings could be well recognized and categorized according to rhombohedral structure of BFO which is a confirmation of phase purity of the sample in agreement with the XRD studies.

3.3 Raman Studies

Raman spectroscopy was employed to further investigate the structural modification in the Zr-doped BFO samples within wave number range $50\text{--}700\text{ cm}^{-1}$ (Fig. 3a). Raman-active modes for rhombohedral structure with $R3c$ space group can be summarized using irreducible presentation $\Gamma_{\text{Raman}} = 4A_1 + 9E$. It is reported that A_1 -1, A_1 -2, A_1 -3, E-1 and E-2 modes are associated with Bi–O covalent bond, whereas higher wave number modes ($>400\text{ cm}^{-1}$) are assigned to Fe–O bond [13]. All the 13 Raman-active modes are present in Zr-doped BFO samples. For $x = 0.03$ sample, the three strong peaks at $138.03, 161.30$ and 204.55 cm^{-1} are designated as A_1 -1, A_1 -2 and A_1 -3 modes, respectively.

Fig. 3 **a** Room temperature Raman spectra of Zr-doped BFO nanoparticles. **b** UV-visible absorption spectra for BFZ nanoparticles



The observed Raman modes for Zr-doped BFO samples are in agreement with the reported data for BFO single crystals [14]. As the Zr concentration increases in $x = 0.03$ and 0.10 samples, the A_1-1 , A_1-2 and A_1-3 modes show no evident peak shifting. This suggests that Zr ions get substituted only on the Fe site and thus does not make any significant change in A_1 modes.

3.4 UV-Visible Studies

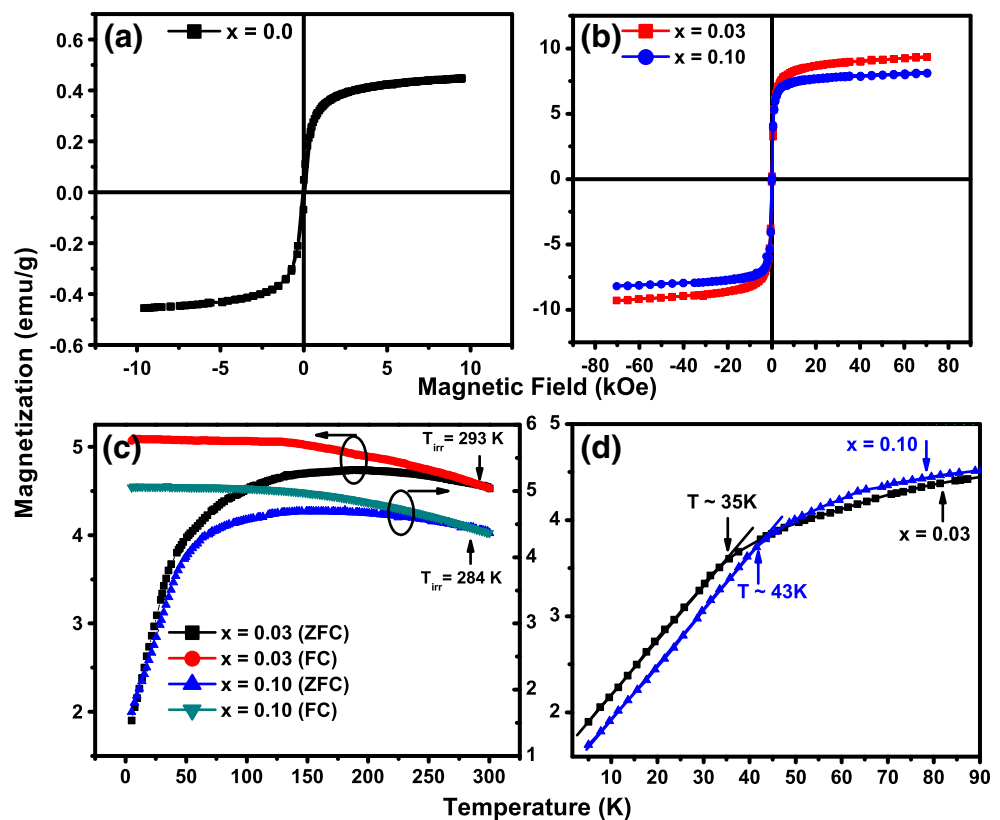
Figure 3b shows the UV-visible diffuse absorbance spectra for pure and Zr-doped samples in the range 1.75–5 eV. For pure BFO sample, three absorption bands are observed, whereas the four absorption bands can be clearly observed for $x = 0.03$ and 0.10 samples. The minority channel dipole-allowed charge transfer excitations give rise to the electronic bands at 3.2 and 4.3 eV [2, 3] for all samples. However, the 3.2 eV band splits into multiplets followed by a low-energy band at 2.5 eV for $x = 0.03$ and 0.10 samples. The splitting of this strongly hybridized O p and Fe d excitations may be attributed to the distorted FeO_6 octahedra and strained nature of Zr-doped BFO nanoparticles [3]. The band gap values as calculated from $(\alpha h\nu)^2$ versus $h\nu$ plots are 2.27, 2.23 and 2.21 eV for $x = 0.0, 0.03$ and 0.10 samples, respectively. Herein, the band gap of

Zr-doped nanoparticles decreased significantly than that of BFO thin films (2.67 eV) [3]. This decrease in band gap may be attributed to the splitting of 3.2 eV charge transfer excitations due to a structural distortion with Zr substitution in BFO lattice. The electronic band at 2.1 eV is assigned to the overlap of ligand field transitions and charge transfer band tail [15].

3.5 Magnetic Studies

The room temperature magnetization-magnetic field ($M-H$) hysteresis curves of the pure and Zr-doped samples are shown in Fig. 4a, b. The $M-H$ curves show large saturation magnetization values of 0.44, 9.33 and 8.14 emu/g for $x = 0.0, 0.03$ and 0.10 samples, respectively. The observed values of remnant magnetization and coercivity are 0.050 emu/g, 73.424 Oe for $x = 0.0$; 0.229 emu/g, 28.577 Oe for $x = 0.03$; and 0.143 emu/g, 17.192 Oe, for $x = 0.10$ sample, respectively. The observed values of saturation magnetization are higher than the reported values for Zr^{4+} -doped BFO [9] and Pr^{3+} - and Zr^{4+} -codoped BFO bulk ceramics [10]. There could be several reasons responsible for ferrimagnetism in Zr-doped samples. First, in the case of nanoparticles surface to volume ratio increases, as a result, the long-range antiferromagnetic order interrupted

Fig. 4 Room temperature $M-H$ curves for **a** $x = 0.0$ sample, **b** $x = 0.03$ and $x = 0.10$ samples, **c** zero-field- and field-cooled curves at 500 Oe for $x = 0.03$ and 0.10 samples. **d** An enlarge view of ZFC curves of $x = 0.03$ and 0.10 samples



at the particle surface due to a cycloid spin structure is suppressed, and the contribution of uncompensated spins at the surface to the total magnetic moment of the nanoparticle increases [1]. Second, the structural distortion induced by Zr substitution in BFO lattice suppressed the spatial spin modulation, resulting in enhanced magnetization. Third, a local ferromagnetic coupling might contribute to enhanced magnetization by replacing time by time some magnetically active Fe^{3+} ions with non-magnetically active Zr^{4+} ions as reported by Wei et al. [9]. However, the saturation magnetization first increases from $x = 0.0$ to $x = 0.03$ sample and then reduces for $x = 0.10$ sample. For $x = 0.10$ sample, the increasing number of non-magnetically active Zr^{4+} ions plays a dominant role for a decrease of magnetization over substitution-induced spiral spin modulation. The formation of Fe–O–Zr coordination (the less magnetic sublattice) could be responsible for the reduction of magnetization for $x = 0.10$ sample.

Magnetization versus temperature curves for an external field of 500 Oe in zero-field-cooled (ZFC) and field-cooled (FC) modes are displayed in Fig. 4c. FC and ZFC modes remain unperturbed until 293 and 284 K for $x = 0.03$ and 0.10 samples, respectively. After which, the bifurcation of FC and ZFC curves gets initiated, i.e. FC mode increases and ZFC mode decreases linearly with temperature. The large difference between FC and ZFC curves was observed which was due to the spin glass-type behaviour. This type of behaviour was previously reported in single crystals of BFO [16]. Spin glass-type behaviour is most dominant in the case of nanoparticles which may be due to the following reasons: (i) reduction in particle size increased surface to volume ratio which induces a large strain in the sample as compared to bulk BFO and (ii) increased in a number of uncompensated Fe^{3+} spins on the surface results in distortion in coordination, and magnetic spin-strain interaction increases [4]. These factors have a remarkable effect on magnetization of the sample. Figure 4d shows the zoom view of the ZFC curves of $x = 0.03$ and 0.10 nanoparticles. The inflection points are obtained at ~ 35 and ~ 43 K for $x = 0.03$ and 0.10 samples, respectively, which are different from the bulk single crystal. In bulk BFO, similar transition was reported at 50 K as a sharp cusp [16]. Shifting of inflection point from 50 K reflects the nanosized nature of Zr-doped BFO samples.

4 Conclusions

In summary, pure and Zr-doped BFO nanoparticles have been successfully prepared by sol-gel method. Obtained XRD patterns and Raman spectra exhibited rhombohedral phase with space group $R3c$ for all the samples. The red shift in the optical band gap of Zr-doped nanoparticles is observed due to distortion in the BFO lattice. The reduction in saturation magnetization for $x = 0.10$ sample is ascribed to the dominance of increasing non-magnetically active Zr^{4+} ions over the suppressed spatial spin modulation.

Acknowledgments This work was financially supported by the Department of Science and Technology (DST), India, through a grant no. SR/FTP/PS-91/2009.

References

- Bhushan, B., Das, D., Priyam, A., Vasanthacharya, N.Y., Kumar, S.: Mater. Chem. Phys. **135**, 144 (2012)
- Chen, P., Xu, X., Koenigsman, C., Santulli, A.C., Wong, S.S., Musfeldt, J.L.: Nano Lett. **10**, 4526 (2010)
- Chen, P., Podraza, N.J., Xu, X.S., Melville, A., Vlahos, E., Gopalan, V., Ramesh, R., Schlom, D.G., Musfeldt, J.L.: Appl. Phys. Lett. **96**, 131907 (2010)
- Jaiswal, A., Das, R., Vivekanand, K., Abraham, P.M., Adyanthaya, S., Poddar, S.P.: J. Phys. Chem. C **114**, 2108 (2010)
- Sen, K., Thakur, S., Singh, K., Gautam, A., Singh, M.: Mater. Lett. **65**, 1963 (2011)
- Gautam, A., Singh, K., Sen, K., Kotnala, R.K., Singh, M.: Mater. Lett. **65**, 591 (2011)
- Chauhan, S., Kumar, M., Chhoker, S., Katyal, S.C., Singh, H., Jewariya, M., Yadav, K.L.: Solid State Commun. **152**, 525 (2012)
- Kumar, M., Yadav, K.L.: J. Appl. Phys. **100**, 074111 (2006)
- Wei, J., Haumont, R., Jarrier, R., Berthet, P., Dkhil, B.: Appl. Phys. Lett. **96**, 102509 (2010)
- Sati, P.C., Arora, M., Chauhan, S., Chhoker, S., Kumar, M.: J. Appl. Phys. **112**, 094102 (2012)
- Arora, M., Sati, P.C., Chauhan, S., Panwar, A.K., Kumar, M.: J. Supercond. Nov. Magn. **26**, 443 (2013)
- Mukherjee, S., Gupta, R., Garg, A., Bansal, V., Bhargava, S.J.: J. Appl. Phys. **107**, 123535 (2010)
- Singh, M.K., Ryu, S., Jang, H.M.: Phys. Rev. B **72**, 132101 (2005)
- Haumont, R., Kreisel, J., Bouvier, P., Hippert, F.: Phys. Rev. B **73**, 132101 (2006)
- He, Y.P., Miao, Y.M., Li, C.R., Wang, S.Q., Cao, L., Xie, S.S., Yang, G.Z., Zou, B.S.: Phys. Rev. B **71**, 125411 (2005)
- Singh, M.K., Prellier, W., Singh, M.P., Katiyar, R.S., Scott, J.F.: Phys. Rev. B **77**, 144403 (2008)